

Seasonal and decadal variations in phytoplankton and non-algal particulate matter absorption in the Northwest Atlantic

Emmanuel Devred^{1,*}, Tim Perry¹ and Philippe Massicotte²

¹*Ocean and Ecosystem Sciences Division, Bedford Institute of Oceanography, Fisheries and Oceans Canada, Dartmouth, NS, Canada*

¹*Département de Biologie, Tukuvik Joint International Laboratory/UMI 3376, ULAVAL (Canada) – CNRS (France), Université Laval, Québec, QC, Canada*

Correspondence*:

Emmanuel Devred

emmanuel.devred@dfo-mpo.gc.ca

2 ABSTRACT

Absorption properties of phytoplankton and non-algal particulate matter were studied in relation to phytoplankton biomass, as indexed by chlorophyll-a concentration, and community structure, as indexed by fucoxanthin concentration, for the Northwest Atlantic using an extensive dataset collected over the last 20 years in all four seasons of temperate latitudes. We found significant differences in the spatio-temporal variations of the bio-optical properties for three oceanic regimes: mesotrophic (Scotian Shelf), oligotrophic(Northwest Atlantic Basin) and sub-artic (Labrador Sea). Variations in the spectral absorption of phytoplankton was related to phytoplankton assemblage as indicated by both changes in fucoxanthin pigment and packaging effect. We also introduced a new index, the phytoplankton apparent absorption wavelength, a weighted sum of absorption expressed in nanometer that provide information on the phytoplankton biomass and assemblage. Time series analysis of the phytoplankton apparent absorption wavelength revealed a decrease of this property in spring on the Scotian Shelf, North Atlantic Basin and Labrador Sea and an increase in autumn on the Scotian Shelf and North Atlantic Basin.

Keywords: Phytoplankton, absorption, chlorophyll-a concentration, phytoplankton apparent absorption wavelength (*PAAW*), Northwest Atlantic, Time series analysis

1 INTRODUCTION

Underwater light characteristics are important drivers of ecological processes. Among others, the magnitude of the primary productivity of photosynthetic communities (Platt and Gallegos, 1980) and the photodegradation of organic matter (Moran and Zepp, 1997) are directly influenced by the quality and quantity of light penetrating the water column. The optically active constituents (OACs) controlling water's inherent optical properties (IOPs), such as light absorption and scattering, in one ecosystem may differ fundamentally from those in another. In open water environments where the optical properties of the ocean are driven by phytoplankton, commonly referred to as case 1 waters (Morel and Prieur, 1977), absorption by phytoplankton and its detrital matter plays a key role in regulating the underwater lightscape as phytoplankton absorption alone represents more than 50% of the total light absorption budget (Oubelkheir et al., 2007; Mascarenhas et al., 2017). An extensive literature has established empirical relationships between water OACs (mostly

chlorophyll-a concentration and associated pigments) and their IOPs in the open oceans (e.g. Gordon and McCluney, 1975; Morel and Bricaud, 1981; Mobley, 1994; Bricaud et al., 1995; Cleveland, 1995; Bricaud et al., 1998; Ciotti et al., 2002; Bricaud et al., 2004; Devred et al., 2006b; Bricaud et al., 2010; Brewin et al., 2011), and coastal (Babin et al., 2003) and polar aquatic environments (Matsuoka et al., 2014; Ferreira et al., 2017). The absorption coefficient of phytoplankton at a given wavelength λ (nm), $a_\phi(\lambda)$ (m^{-1}), has often been used as a proxy for phytoplankton biomass (Roesler and Barnard, 2013; Nardelli and Twardowski, 2016). It is also known to be highly influenced by the growing conditions and the physiological state of the algal assemblage and may not always truly represent the carbon content of phytoplankton cells (Behrenfeld et al., 2006). Phytoplankton absorption magnitude and spectral dependence also inform on phytoplankton community structure (Hirata et al., 2008) and have been used in primary production models, either directly to retrieve production (Marra et al., 2007) or indirectly to weight phytoplankton light harvesting efficiency (Morel, 1978; Kyewalyanga et al., 1997). Along with a_ϕ , the chlorophyll-specific absorption coefficient (a_ϕ^* , absorption per unit concentration of chlorophyll-a in $\text{m}^2 \text{ mg}^{-1}$) varies with changes in phytoplankton intracellular composition and concentration, and pigment packaging effect (Duygens, 1956; Mitchell and Kiefer, 1988; Kirk, 1976; Bricaud et al., 1995, 2004). The exploitation of these features has led to the determination of phytoplankton size classes and taxonomic groups in natural water samples using optical satellites (Ciotti et al., 2002; Devred et al., 2006b, 2011; Fujiki and Tagushi, 2002; Sathyendranath et al., 2004; Brewin et al., 2011). Because phytoplankton absorption is characterized by a wide peak around 443 nm and a sharp maximum around 675 nm, empirical relationships usually focus on these two wavelengths rather than fully exploiting the spectral information contained in absorption measurements (Babin et al., 2003; Bricaud et al., 1995; Aiken et al., 2007). Still, these indices have been proven useful to study the phytoplankton dynamics in aquatic ecosystems. Absorption by non-algal particles, a_{NAP} (m^{-1}), a “methodological by-product” of the determination of phytoplankton absorption derived from total particulate absorption, a_p (m^{-1}), has been less studied than phytoplankton absorption even if its role in shaping the underwater lightscape is not negligible. Its spectral resemblance to the colored dissolved organic matter absorption spectrum has often resulted in lumping both absorptions together when solving radiative transfer problems (Hoge and Lyon, 1999; Maritorena et al., 2002; Devred et al., 2006a; Werdell et al., 2018). Bricaud et al. (1998) found a significant relationship between chlorophyll-a concentration and a_{NAP} , however the relationship between these two variables may be location-dependent (Sosik and Mitchell, 1992). The ratio between a_p and a_{NAP} has been found to be as low as 10% at the surface in open oceans and reach 20% to 30% at depth (Bricaud et al., 1998), while it can dominate the absorption budget in coastal areas (Babin et al., 2003; Williams et al., 2018; Kratzer and Moore, 2018).

Long-time series of *in situ* measurements at high spatial resolution are difficult to acquire due to financial and logistical constraints. Hence, samplings in ecological studies are often carried out at a single location over a short period of time focusing on a single process such as the algal spring bloom event, or by combining data from various field campaigns that were carried out in different locations and times (Bricaud et al., 2004; Devred et al., 2006b), which hinder our understanding of the seasonal dynamics of phytoplankton absorption. In the current study, we used an extensive and comprehensive dataset acquired within the Atlantic Zone Monitoring Program (AZMP Casault et al., 2020) and Atlantic Offshore Zone Monitoring Program (AZOMP Yashayaev et al., 2021) frameworks made of water samples collected over the last 20 years to describe in details the seasonal variability of chlorophyll-a concentration ([Chl-a] in mg m^{-3}), a_ϕ and a_{NAP} as well as their relationships in three regions of the Northwest Atlantic. We also used information on fucoxanthin concentration ([Fucox] in mg m^{-3}) as an indicator of diatom presence to help interpret the results. We addressed the challenge of using hyperspectral information, namely phytoplankton absorption, in environmental studies to determine the status of the marine ecosystem given

73 its complex interpretation due to its large variation over the visible spectrum, such that the use of only
74 one or two wavelengths truncates the information contained in an entire spectrum. We present a simple
75 absorption index for phytoplankton absorption (i.e., Phytoplankton Apparent Absorption Wavelength,
76 *PAAW*) that was inspired by the work of Vandermeulen et al. (2020) who applied this concept to remote
77 sensing reflectance. This index summarizes all the spectral information contained in a given phytoplankton
78 absorption spectrum into a single number (nm) that provides information on the biomass and structure of
79 the phytoplankton community bypassing the need for chlorophyll-a concentration measurements. Our large
80 dataset provided the ability to detect possible changes in *PAAW* at the regional scale over two decades
81 and to test the minimum sampling requirement to capture the natural variability of the Northwest Atlantic
82 ecosystem.

2 MATERIAL AND METHODS

83 2.1 Study area and sampling

84 Since 1999, the Department of Fisheries and Oceans Canada (DFO) conducts annual surveys in the
85 Northwest Atlantic as part of the Atlantic Zone and Atlantic Offshore Zone monitoring programs (Theriault
86 et al., 1998; Pepin et al., 2005). Each year, in spring, sometimes between April and June depending on ship
87 availability and weather, about 100 stations are sampled on the Scotian Shelf and Gulf of Maine region and
88 28 stations are sampled in the Labrador Sea along a transect that spans from the Labrador Shelf (Canada) to
89 the Greenland Shelf (Denmark), crossing the Labrador Basin (Figure 1). The spring cruise on the Scotian
90 Shelf is repeated in the autumn from mid-October to mid-November. Fish surveys that happened during
91 winter and summer opportunistically provided additional water samples. For this study, a total of 3279
92 sampling events were compiled and grouped into three bioregions, namely the Scotian Shelf, a temperate
93 mesotrophic environment, the Northwest Atlantic Basin, and a temperate oligotrophic environment and
94 the Labrador Sea, a sub-arctic environment (See Supplementary Figure S1 for details on samples spatio-
95 temporal distribution). The delineation of these bioregions was based on bathymetry (GEBCO2021) and
96 the latitude: (1) Scotian Shelf (bathymetry < 600 m and latitude < 48°N), (2) Northwest Atlantic Basin
97 (bathymetry ≥ 600 m and latitude < 48°N) and (3) Labrador Sea (latitude ≥ 48°N). Observations were
98 further grouped into seasons based on the time of sampling (Supplementary Figure S1B): spring (Mar,
99 Apr, May, $N = 1598$), summer (Jun, Jul, Aug, $N = 369$), autumn (Sept, Oct, Nov, $N = 1174$) and winter
100 (Dec, Jan, Feb, $N = 138$). At each station, surface water (< 30 m) was collected to measure phytoplankton
101 pigment composition and particulate absorption.

102 2.2 Data and laboratory analysis

103 2.2.1 Chlorophyll-a and Fucoxanthin pigment concentration

104 Samples for pigment analysis were filtered at low pressure (< 10 dpi) on 25 mm WF/F Whatman filters
105 (sterile Grade F Glass microfiber) with 0.2 μm mesh size and immediately flash frozen and stored in
106 Nitrogen Liquid during the sea-going fieldwork. The volume of filtration varied between 0.25 and 1 L
107 based on a visual inspection of the filter colour to ensure that enough material was retained for analysis.
108 Upon return to the Bedford Institute of Oceanography, the samples were stored inside a -80° C freezer until
109 analysis in the laboratory. Pigments composition and concentration were measured on a Beckman–Coulter
110 Gold High-Performance Liquid Chromatography (HPLC) system between 1998 and 2013, and on an
111 Agilent 12000 HPLC system for samples collected between 2013 and 2020. Details on the HPLC method
112 to extract and measure pigment concentration can be found in Head and Horne (1993). In this study, we
113 limited the pigments to chlorophyll-a and derivative ([Chl-a] in mg m^{-3}) and fucoxanthin ([Fucox] in mg
114 m^{-3}) concentration, the latter being used as a coarse indicator of diatom presence in samples.

115 2.2.2 Absorption coefficient of phytoplankton and non-algal particulate matter

116 Filtration for phytoplankton (a_ϕ) and non-algal particles (a_{NAP}) absorption coefficients were carried
 117 out simultaneously than the filtration for pigment analysis following the same protocol (i.e., filtration
 118 and storage method). Phytoplankton absorption coefficients between 350 and 750 nm were measured at
 119 1 nm increment on a UV-Vis Shimadzu 2600i double beam with an integrating sphere in transmission
 120 mode. Only the visible part of the spectrum (400-700 nm) was used in the current study. Total particulate
 121 absorption coefficient (a_p) was measured first, after which, the filter was soaked in hot methanol for 25
 122 to 45 minutes to extract phytoplankton pigments. The absorption by non-algal particles, also referred
 123 to as detritus absorption, was then measured, and phytoplankton absorption was inferred by subtraction
 124 of a_{NAP} to a_p as described in Mitchell and Kiefer (1984) following modifications by Hoepffner and
 125 Sathyendranath (1991) and Kyewalyanga et al. (1997). The pathlength correction (i.e., the β -factor) was
 126 computed as in Stramski et al. (2015). Two quality control procedures were used to ensure the integrity
 127 of the absorption dataset; spectra were removed from further analysis if: (1) negative values occurred
 128 between 350 and 400 nm and (2) the absorption coefficient at 410 nm was higher than the one at 443 nm
 129 as in Devred et al. (2006b). The slope of the exponential decrease of the particulate absorption spectrum,
 130 S_{NAP} , was computed by fitting equation 1 to the data using the *nls()* function in R over the range 400 to
 131 700 nm excluding the 400 to 480 nm and 620 to 700 nm ranges to avoid possible contamination by pigment
 132 remaining from the extraction:

$$a_{NAP}(\lambda) = a_{NAP}(443)(-S_{NAP}(\lambda - 443)). \quad (1)$$

133 2.3 Statistical Analysis

134 2.3.1 Phytoplankton apparent absorption wavelength

135 To summarize the spectral information contained in phytoplankton absorption measurements in a simple
 136 index, we used a method similar to that of Vandermeulen et al. (2020). The formulation of this index was
 137 initially proposed to maximize the utilization of the spectral information contained in remote sensing reflec-
 138 tance, and simply represents the weighted harmonic mean of a spectrum. As pointed out by Vandermeulen
 139 et al. (2020), the index indicates the wavelength balance point around which the absorption spectrum is
 140 evenly distributed. Since we adopted this index to characterize the spectral shape of in situ phytoplankton
 141 absorption, we named it the phytoplankton apparent absorption wavelength ($PAAW$, nm), which was
 142 calculated as follows:

$$PAAW = \frac{\sum_{\lambda=400}^{\lambda=700} a_\phi(\lambda)}{\sum_{\lambda=400}^{\lambda=700} a_\phi(\lambda)/\lambda} \quad (2)$$

143 Where $a_\phi(\lambda)$ is the phytoplankton absorption coefficient at the wavelength λ (nm).

144 2.3.2 Regression and trend analysis

145 The relationship between the phytoplankton absorption coefficient at a given wavelength and [Chl-a] was
 146 derived using a type-2 linear regression on the log10-transformed data (when required to achieve normality).
 147 Times series analysis of the $PAAW$ were performed on data collected in spring and autumn only (except
 148 for the Labrador Sea in autumn), as there were no sufficient years with data in winter and summer to obtain
 149 statistically reliable trends. For the nine time series, namely the entire dataset, the three datasets partitioned
 150 into regions and the five datasets partitioned into seasons and regions, the mean $PAAW$ were computed
 151 and its trend was derived using a weighted linear model (*lm()* in R). The weights for the fit were derived

152 using the number of data available in any given year/region/season. The slope of the linear regression of
153 the mean *PAAW* was used to describe the trend.

3 RESULTS

154 3.1 [Chl-a], [Fucox], absorption coefficients and *PAAW* seasonal and regional 155 variations

156 For the three biogeochemical regions, both mean [Chl-a] and [Fucox] were highest in spring when
157 phytoplankton bloom and the community assemblage is dominated by diatoms with values of 2.70, 1.80
158 and 2.73 mg m⁻³ for [Chl-a] on the Scotian Shelf, NAB and the Labrador Sea, respectively, and values of
159 0.89, 0.47 and 0.72 mg m⁻³ for [Fucox] on the Scotian Shelf, NAB and the Labrador Sea, respectively
160 (Table 1). The Scotian Shelf showed the highest seasonal variability with a strong decrease of both [Chl-a]
161 and [Fucox] in summer followed by an increase during autumn and a second decrease in winter for [Chl-a]
162 that remained higher than the mean summer values, while [Fucox] in winter was greater than in autumn
163 (Figure 2). Both [Chl-a] and [Fucox] in NAB followed the same seasonal pattern as on the Scotian Shelf,
164 but with smaller mean values. The Labrador Sea exhibited a different seasonal cycles than the two other
165 regions, as both [Chl-a] and [Fucox] continuously decreased during summer, autumn and winter to reach
166 the lowest values of all regions and seasons (i.e., [Chl-a] = 0.19 mg m⁻³ and [Fucox] = 0.05 mg m⁻³). The
167 similar seasonal cycle between [Chl-a] and [Fucox] is supported by the high degree of correlation between
168 the two pigments ($R^2 = 0.85$, Figure 3)

169 As for [Chl-a] and [Fucox], the absorption coefficients at 443 nm for particulate matter, non-algal particule
170 and phytoplankton spanned about three orders of magnitude and followed a normal distribution when
171 log₁₀-transformed (Figure S2). All properties showed large regional and seasonal variabilities (Table 1
172 and figure 2). Data revealed the same seasonal cycle for $a_\phi(443)$ than for [Chl-a] with the exception that
173 $a_\phi(443)$ was slightly higher in the autumn (0.059 m⁻¹) than in the spring (0.050 m⁻¹) on the Scotian Shelf
174 (Table 1). The absorption coefficient at 675 nm (Figure 2B) exhibited the same seasonal cycle as $a_\phi(443)$
175 with smaller values as expected (Figure 2A and B). The specific absorption coefficient at 443 nm (Figure
176 2C) showed an inversed pattern to [Chl-a] and $a_\phi(443)$ in all regions, perhaps with less variability between
177 summer and autumn on the Scotian Shelf compare to $a_\phi(443)$ and the notable exception of the low mean
178 $a_\phi^*(443)$ in the Labrador Sea when [Chl-a] is also low. The absorption coefficient at 443 nm by non-algal
179 particulate matter exhibited a different seasonal pattern than $a_\phi(443)$ on the Scotian Shelf, with high values
180 reached in the spring followed by a decrease in summer and an increase for both autumn and winter (Figure
181 2D). In the NAB, $a_{NAP}(443)$ was highest in spring, with values relatively low (0.0051 m⁻¹) compared
182 to the Scotian Shelf (0.009 m⁻¹) and Labrador Sea (0.0075 m⁻¹). For the rest of the year, $a_{NAP}(443)$
183 remained quasi constant with values of about 0.0035 m⁻¹ (ANOVA test p-value < 0.05). In the Labrador
184 Sea, $a_{NAP}(443)$ showed a similar seasonal pattern to $a_\phi(443)$ with a continuous decrease from spring to
185 winter, unlike the two other regions where markedly different seasonal patterns were observed. The slope
186 of the *NAP* absorption spectrum also shows very weak seasonal dependence (Figure 2E), with a slight
187 decrease from spring to winter on both the Scotian Shelf and NAB, while S_{NAP} reaches a minimum in
188 autumn in the Labrador Sea.

189 The *PAAW* provided additional information than [Chl-a], $a_\phi(443)$ and $a_\phi^*(443)$ (Figure 2F). The overall
190 *PAAW* for the Northwest Atlantic was 478 nm (Table 1). On the Scotian Shelf, *PAAW* exhibited a
191 seasonal cycle that resembled the one of $a_\phi^*(443)$ with a mean value of 482.5 nm in Spring that decreased
192 to 470.2 nm in Summer to increase again in autumn (477.5 nm) and winter (480.9 nm). The spring season
193 on the Scotian Shelf exhibited the highest range of variation in *PAAW* of all regions/seasons with about

194 40 nm in variation from 461.6 to 500 nm. In the NAB, *PAAW* followed a similar pattern to $a_\phi(443)$ and
 195 $a_\phi(675)$; *PAAW* in all seasons being smaller than the *PAAW* observed on the Scotian Shelf. Interestingly,
 196 the *PAAW* in the Labrador Sea showed a different pattern than the $a_\phi^*(443)$ and $a_\phi(443)$ ones, associated
 197 with the lowest seasonal variability (477.7 nm in Summer to 481.5 nm in Spring). The *PAAW* was highest
 198 in spring and lowest in winter, while summer and autumn exhibited similar values.

199 3.2 Bio-optical relationships: [Chl-a], $a_\phi(443)$, $a_{NAP}(443)$ and S_{NAP}

200 The [Chl-a]: $a_\phi(\lambda)$ is arguably the most studied of all the bio-optical properties. When grouping all the
 201 data together, independently of regions and seasons, the linear regression of $a_\phi(443)$ against [Chl-a] in the
 202 log₁₀ space can be described in the linear space as:

$$203 \quad a_\phi(443) = 0.0407[\text{Chl-a}]^{0.515}, \quad (3)$$

203

204 The coefficient of the power-law fit provided a factor close to the one found by Bricaud et al. (1998)
 205 (Figure 4A) who reported a value of 0.0378, but with a smaller exponent (Bricaud et al., 1998, i.e., 0.627
 206 in)). Bricaud et al. (2004) derived coefficients of 0.0654 and 0.728 for the factor and exponent, respectively,
 207 for the [Chl-a]– $a_\phi(443)$ relationship, which were larger than the ones found here. The correlation coefficient
 208 in the current study is much smaller than the ones found by Bricaud et al. (1998, 2004), which were equal to
 209 0.90 and 0.93 respectively, which is explained by the linear scale used in their studies, while the R^2 in the
 210 current study was computed on log₁₀-transformed data. The relationship found here remained consistent
 211 with the one found by Devred et al. (2006b), which was established using some of the data included in the
 212 current study. In general, all models agreed well in the bulk range of [Chl-a] between 0.3 and 5 mg m⁻³ and
 213 discrepancies between models occurred mainly in the extreme range of values. The regional relationships
 214 exhibited a large difference in the exponent with values of 0.469, 0.508 and 0.616 for the Scotian Shelf,
 215 NAB and the Labrador Sea respectively, while the intercept in the log₁₀ space remained similar and varied
 216 between -1.37 and -1.42 (corresponding to 0.038 to 0.042 in the linear space) for the three regions (Figure
 217 4C-D). The Scotian Shelf showed the lowest R^2 , with a value of 0.53 that may be driven by seasonal
 218 variations. As for the [Chl-a]– $a_\phi(443)$ relationship, the $a_{NAP}(443)$ – $a_\phi(443)$ relationship showed regional
 219 differences in all three regions, but with $a_\phi(443)$ dominating systematically the particulate absorption
 220 (Figure 5). High variability around the model was consistent with low correlation coefficients, in particular
 221 on the Scotian Shelf. The slope of the linear regression of $a_{NAP}(443)$ against $a_\phi(443)$ was 0.73 ($R^2=0.32$),
 222 0.59 ($R^2=0.23$) and 0.66 ($R^2=0.31$) for the Scotian Shelf, Northwest Atlantic Basin and Labrador Sea
 223 respectively.

224 It has been shown that the sum of diagnostic pigments (i.e., pigments that are used as taxonomic group
 225 markers such as peridinin, fucoxanthin, zeaxanthin and chlorophyll-b) are highly correlated with [Chl-a]
 226 (Claustre, 1994; Vidussi et al., 2001; Uitz et al., 2006). [Fucox] was strongly correlated to [Chl-a] with a
 227 slope of X ($R^2 = Y$) in agreement with previous work (Claustre, 1994)

228 3.3 Spectral variation in phytoplankton absorption

229 A simple method to analyse the spectral variation of phytoplankton absorption relies on the study of
 230 $a_\phi(443)$: $a_\phi(675)$ ratio as a function of [Chl-a], which provides a rapid assessment of the packaging effect
 231 and therefore a rough estimation of community structure (Bricaud et al., 2004; Devred et al., 2006b;
 232 Vishnu et al., 2018). At the Northwest Atlantic scale, both [Chl-a] and [Fucox] were both highly correlated
 233 to $a_\phi(443)$: $a_\phi(675)$ with R^2 of 0.72 and 0.76 respectively (Figure S3). The slope of the regression of
 234 log₁₀-transformed $a_\phi(443)$: $a_\phi(675)$ against [Chl-a] was 0.21 (results not shown). The slope of the regression

235 was lower in the Labrador Sea (i.e., 0.165) compared to the other two bio-regions (0.219 and 0.231 for the
236 Scotian Shelf and Northwest Atlantic Basin respectively, Figure 6). [Chl-a] was slightly more correlated
237 with $a_\phi(675)$ ($R^2 = 0.89$) compared to $a_\phi(443)$ ($R^2 = 0.81$) hinting that other pigments might contribute to
238 absorption in the blue part of the absorption spectrum.

239 Another way of summarising spectral variation in phytoplankton absorption is to use the *PAAW* (see
240 section 2.3.1), which accounts for contribution from all wavelengths rather than only two (i.e., 443 and
241 675 nm). The *PAAW* showed that the spectral shape of the phytoplankton absorption varied across the
242 three bio-regions (Figure 7). For the three regions, a large *PAAW* corresponds to normalized spectra with
243 the flattest shape, where the difference between the blue and red absorption peak is the smallest (Figure
244 7A). As the *PAAW* decreases, phytoplankton in the blue part of the spectrum increases and a shoulder
245 occurs around 490 nm. The Scotian Shelf showed the highest variability in *PAAW* with some of the
246 “bluest” waters with *PAAW* as high as 500 nm (Figure 7B). The distribution of *PAAW* on the Scotian
247 Shelf shows a bimodal shape centered on about 482 nm with a second small bump located around 492 nm,
248 likely the contribution from the summer samples. The Labrador Sea region exhibited the narrowest range
249 of variation for the *PAAW* index, with a mean value and distribution similar to the Scotian Shelf. Finally,
250 the NAB region also followed a normal distribution of the *PAAW*, which was centred on 476 nm and
251 corresponded to the smallest *PAAW* of the three regions. The mean *PAAW* shows that phytoplankton
252 absorption spectra were slightly more shifted in the blue part of the spectrum on the Scotian Shelf and the
253 Labrador Sea compared to the spectra measured in the Northwest Atlantic Basin. *PAAW* was positively
254 correlated to [Chl-a] and negatively ($a_\phi^*(443)$) (Figure 8A and B). A second-order polynomial equation
255 was used to model the decrease of the $a_\phi(443):a_\phi(675)$ ratio with increasing *PAAW* (Figure 8C). High
256 values of *PAAW* were associated with low values of the ratio in the spring. A high spread in the data
257 occurred at low *PAAW* (Figure 8C). The variance in [Chl-a] was slightly better explained by *PAAW* (R^2
258 = 0.69) than by $a_\phi(443)$ (Figure 4, $R^2 = 0.65$). Using *PAAW* to predict $a_\phi(443):a_\phi(675)$ ratio compared
259 to [Chl-a] increased R^2 from 0.72 to 0.87 (Figure 8C). The *PAAW* seasonal cycles in all three regions
260 was very similar to the seasonal cycle of $a_\phi(443):a_\phi(675)$ (Figure S4).

261 Trend analysis of the *PAAW* for the entire dataset and all regions did not show any significant changes,
262 all the trends were positive but with a p-value that remained high (why are you not using weight-averaged
263 results as requested?). However, trend analysis at the regional and seasonal level revealed a significant
264 increase in the *PAAW* in all three regions in spring (Table 2 and Figure 9). The Scotian Shelf exhibited
265 the highest rate of change with a slope of 0.38 nm y^{-1} followed by the Labrador Sea (0.25 nm y^{-1}) and the
266 NAB (0.18 nm y^{-1}). The autumn showed an opposite trend a decrease in the *PAAW* on both the Scotian
267 Shelf (-0.15 nm y^{-1}) and the NAB (-0.31 nm y^{-1}), while there were no sufficient years to compute reliable
268 statistics in the Labrador Sea in Autumn and all regions in Summer and Winter.

4 DISCUSSION

269 In the current study, we have used an extensive dataset of several bio-optical parameters, measured in space
270 and time, to examine their variability and linkage. In general, our results agreed, and reinforced, current
271 knowledge about phytoplankton biomass and community structure, depicted using [Fucox] as a very rough
272 indicator of diatom presence, and their relationships to phytoplankton and non-algal particulate absorptions.
273 The added value of our current study relies upon the quantification of the spatio-temporal variations in
274 bio-optical properties and their trends at the decadal scale. While most studies relies on a single cruise
275 (Stuart et al., 2000; Pérez et al., 2021), a combination of cruises gathered from one region (Ferreira et al.,
276 2013; Matsuoka et al., 2014) or the global ocean without a pre-defined temporal strategy (Trees et al.,
277 2000; Ciotti et al., 2002; Bricaud et al., 2004; Brewin et al., 2011), the DFO monitoring cruises have

278 systematically carried out measurements of bio-optical properties at about 150 stations spanning about 20°
279 in latitudes (i.e., 42 to 62°N) in the NWA and covering the entire seasonal cycle for more than 20 years.
280 The NWA was divided into three regions with markedly different regimes: 1) The Scotian Shelf showed
281 a regime of a mid-latitude shelf environment, with high seasonal variations in phytoplankton biomass
282 and associated properties, 2) the NAB showed the dynamic of an oligotrophic environment, with low
283 biomass compare to the two other regions and a more subtle seasonal cycles and finally 3) the Labrador Sea
284 exhibited the characteristics of a sub-arctic environment with a delayed spring growth in phytoplankton
285 biomass compared to the Scotian Shelf (Wu et al., 2008) that remained sustained over the summer to
286 slowly decrease in autumn and reach low levels in winter when light and sea ice are limiting factors to
287 phytoplankton production. The impacts of these various regimes on the bio-optical properties of the NWA
288 are discussed in the following sections.

289 **4.1 Phytoplankton biomass and absorption in the Northwest Atlantic**

290 The coefficients of the power-law that expressed $a_\phi(443)$ as a function of [Chl-a] (Eq. 3.2) were consistent
291 with previous studies, the main differences occurred in the extreme ranges of the relationship and can
292 be attributed to the range of variations of the bio-optical properties and the type of water sampled in
293 previous studies. For instance, the higher coefficients found by Bricaud et al. (2004) compared to the
294 current study can be explained by the oligotrophic waters that were sampled in their study. This is also
295 highlighted in the regional differences that we found between the three regions of the Northwest Atlantic
296 as emphasized by Stuart et al. (2000) who showed that diatom-dominated waters of the Labrador Sea
297 exhibited a lower absorption coefficient per unit of [Chl-a] than water dominated by prymniesophytes. This
298 led to the development of satellite-based algorithms to identify diatom occurrence in the Northwest Atlantic
299 (Sathyendranath et al., 2004). Seasonal changes in irradiance reaching the water surface, temperature and
300 nutrient availability are among the main drivers that regulate the size structure, the intracellular pigment
301 composition and the absorption characteristics of the algal populations (Ciotti et al., 2002; Bricaud et al.,
302 2004; Churilova et al., 2017). The spring bloom in the NWA is dominated by diatoms in all three regions as
303 suggested by the low specific absorption and high [Fucox] observed during that time (Table 2), in agreement
304 with phytoplankton enumeration carried out at a fixed station on the Scotian Shelf (Casault et al., 2020).
305 The autumn bloom on the Scotian Shelf and in the NAB exhibited $a_\phi^*(443)$ that were much higher than
306 during the spring, despite relatively high phytoplankton biomass, suggesting that large phytoplankton other
307 than diatoms (e.g., dinoflagellates) dominated the phytoplankton assemblage and were associated with
308 low packaging effect (Figure 2C and Table 1). Species succession in the Labrador Sea showed a different
309 pattern with a continuous decrease (increase) of phytoplankton biomass ($a_\phi^*(443)$). While high biomass
310 and dominance of diatoms have been established in spring in the Labrador Sea using both phytoplankton
311 counts and pigment composition (Fragoso et al., 2017, 2018), the present study reveal for the first time the
312 entire annual cycle of phytoplankton assemblage based on optical traits with large cells dominating the
313 spring and summer signal while small cells dominated the optical signal in autumn and winter. Although
314 no direct measurements of the phytoplankton cell size were made during the DFO oceanographic cruises, a
315 rich literature has demonstrated that inferences of cell size could be made from IOPs. For instance, results
316 from Fujiki and Tagushi (2002) indicated that a decrease in $a_\phi(675)$ was solely associated with increasing
317 phytoplankton cell volume and packaging effect. Likewise, Bricaud et al. (1995) found that increase in
318 [Chl-a] was negatively correlated with both $a_\phi^*(443)$ and the blue-to-red phytoplankton absorption ratio (see
319 Figure 8C) that was further attributed to an increasing pigment packaging and lower proportion of accessory
320 pigments (Staehr et al., 2004; Vishnu et al., 2018). Here we found a decrease of the $a_\phi^*(443) : a_\phi^*(675)$
321 with [Fucox] for the entire dataset with a slope of -0.163 (Figure S3) in the log₁₀-space (0.23 in the linear
322 space), which is consistent with the results of Hoepffner and Sathyendranath (1993) who found an increase

of $a_\phi(440) : a_\phi(550)$ with [Fucox] from 0.05 to 0.3 depending on the phytoplankton assemblage. While Hoepffner and Sathyendranath (1993) used a different phytoplankton absorption ratio, the results point in the same direction of the change in phytoplankton spectral shape with changes in phytoplankton community structure.

Spatio-temporal variations of non-algal particulate absorption magnitude and spectral dependence showed complex patterns (Figure 2E and F). The dataset encompassed a wide range of variations in both $a_{NAP}(443)$ and S_{NAP} certainly due to the type of water sampled, which included mesotrophic coastal environments on the Scotian Shelf, oligotrophic waters of the NAB and sub-arctic waters of the Labrador Sea. However, several patterns emerged at the regional scale, $a_{NAP}(443)$ remained below 11% of $a_\phi(443)$ in general, with the highest percentage observed in the mesotrophic environment of the Scotian Shelf and the lower values occurring in the NAB (Table 1). Large discrepancies were observed around the mean relationship (Figure 5) suggesting that many short-term processes may be included in the production of detritus from living phytoplankton (i.e., grazing, viral lysis) that were captured by the repeated sampling. However, only a study at high temporal frequency sampling (i.e., several times a day for several days) may reveal the processes included in the degradation of phytoplankton and lead to a detailed understanding of the absorption dynamics of phytoplankton and non-algal particles. Diatom-dominated phytoplankton biomass, as indicated by [Fucox], was associated with high $a_{NAP}(443)$ and high S_{NAP} (Table 1). For instance, relatively high [Chl-a] and [Fucox] on the Scotian Shelf (2.7 and 0.89 mg m⁻³, respectively) and Labrador Sea (2.7 and 0.72 mg g⁻³, respectively) in spring were associated with high $a_{NAP}(443)$ (0.009 and 0.0075 m⁻¹ for the Scotian Shelf and Labrador Sea, respectively) and S_{NAP} (0.0124 and 0.0134 m⁻¹ for the Scotian Shelf and Labrador Sea, respectively). On the other hand, low [Chl-a] and [Fucox] in the NAB in summer were associated with low $a_{NAP}(443)$ and S_{NAP} . A departure from this pattern was the high [Chl-a] and low [Fucox] associated with relatively low $a_{NAP}(443)$ and S_{NAP} on the Scotian Shelf in autumn. Magnitude and spectral absorption by detritus may depends on the phytoplankton assemblage and its degradation through biogeochemical processes (e.g., virus infection, Nagasaki, 2008). The spring bloom also corresponds to the maximum of zooplankton abundance on the Scotian Shelf (Casault et al., 2020) and a number of studies have demonstrated the selective feeding of zooplankton towards diatoms (Teegarden et al., 2001; Leising et al., 2005). Grazing by zooplankton produces phaeopigments (Shuman and Lorenzen, 1975; Head and Horne, 1993; Collos et al., 2005) and increases the concentration of detritus (i.e., non-algal particles) in the water column and therefore its absorption. These processes suggest that the spectral slope of the absorption by NAP might be impacted by community structure and zooplankton grazing, however, this statement would need to be further studied. Our results, however, support that zooplankton grazing may have an impact on the bulk optical properties of seawater and the emergence of new sensors with hyperspectral capability may help inform secondary production using variation in a_{NAP} as an indicator of zooplankton grazing activity.

4.2 The phytoplankton apparent absorption wavelength (PAAW): an integrative index of the spectral shape of phytoplankton absorption

Retrieval of pigments concentration from absorption spectrum has been carried out in the past using gaussian decomposition (Hoepffner and Sathyendranath, 1991; Chase et al., 2013; Zhang et al., 2021), machine learning (Chazottes et al., 2006; Bricaud et al., 2007) and derivative analysis (Bidigare et al., 1989; Catlett and Siegel, 2018) to cite a few methods. Here we used an integrative index and related it to phytoplankton bio-optical properties. The takeaway message from this index is that it performed slightly better, in terms of R^2 , than any other variable, namely [Chl-a], [Fucox], $a_\phi(443)$ and $a_\phi^*(443) : a_\phi^*(675)$ when studying the triangular relationship between absorption, biomass and community structure. The PAAW provided information on the trophic status as supported by the high correlation coefficient with

[Chl-a] ($R^2=0.66$), which was similar to the [Chl-a]– $a_\phi(443)$ one ($R^2=0.65$). The other advantage of the *PAAW* that it can also be used to describe the community structure given its high correlation to $a_\phi(443) : a_\phi(675)$ ($R^2 = 0.88$) and [Fucox] ($R^2 = 0.69$). Analysis of the phytoplankton absorption spectral variation showed consistency with *PAAW* and notably, non-linear changes in the absorption spectra from small-cell to large-cell that translated into a decrease in *PAAW* (Figure 8C). Another advantage of the *PAAW* is that its variation on a linear scale, compare to other bio-optical parameters that are expressed on a \log_{10} scale, makes it a valuable index to report on changes in the environment and support decision making. For instance, the *PAAW* could be used for long-term monitoring, as shown by our time series analysis. Seasonal and regional analysis of *PAAW* revealed a shift in phytoplankton biomass in Spring towards smaller *PAAW* (e.g., blue) suggesting a decrease in the packaging effect and abundance of large phytoplankton such as diatoms. This is consistent with a recent satellite-based study that reveals an overall decrease in large phytoplankton in the biogeochemical provinces of the Northwest Atlantic (Liu et al., 2018). An opposite trend was observed in the autumn on the Scotian Shelf and NAB with a shift of *PAAW* toward the green wavelength, the shift was particularly important in the NAB. The *PAAW* might be a better indicator than [Chl-a] to study the impact of climate change on phytoplankton biomass and community structure as (Dutkiewicz et al., 2019) demonstrated that changes in watercolour, as indicated by remote sensing reflectances, is a better indicator of changes in phytoplankton regimes as it includes information on changes in community structure. The *PAAW*, an index that accounts for both phytoplankton biomass and community structure, is easily understandable by a non-expert and provides valuable information on the phytoplankton regime in the marine ecosystem.

4.3 How many measurements do we need to characterize the bio-optical dynamics of an ecosystem?

Sampling the ocean to study a given phenomenon (e.g., phytoplankton spring bloom) can be challenging given logistic constraints (e.g., ship availability, weather) and the inherent temporal variation of ocean processes. Long-term monitoring programs with dates set in advance mitigate challenges as the repetitive measurements in space and time ensure that most oceanographic conditions will be encountered over years of field measurements. In the case of the spring bloom on the Scotian Shelf, given its variability in time (initiation varies over several weeks) and patchiness, the AZMP spring missions have sampled in many instances ante-, per- and post-bloom conditions as indicated by the wide range of [Chl-a] measured (0.1 to 13 mg m^{-2}). The-optical relationships found in our study were in agreement with previous models (see section 3.2) emphasizing the universality of such relationships while supporting also the need to account for regional characteristics for fine-tuning. Our results explains the good performance of global algorithms such as the Ocean Land Colour Imager (OLCI) Neural Network [Chl-a] algorithm (Hieronymi et al., 2017) or the QAA algorithm (Lee et al., 2002), which development relied on radiative transfer simulation that included the absorption models of Bricaud et al. (1995, 1998, 2004).

Long-term monitoring programs are needed to characterize trends and shifts in ecosystems, however, one can wonder to what effort sampling is needed to characterize the variability within an ecosystem. We addressed this question here by plotting the cumulative mean and standard deviation (SD) as a function of time for [Chla], $a_\phi(443)$, $a_{NAP}(443)$ and S_{NAP} (Figure 10), assuming that when SD reaches an asymptotic value, the variability of the ecosystem has been described. Our results suggest that about 5 years of sampling in spring and autumn on the Scotian Shelf were sufficient to capture the variability in $a_{NAP}(443)$, while about 10 years were necessary for the autumn. Standard deviations in [Chl-a] and $a_\phi(443)$ reached their asymptotic values after 10 years. After 20 years of data collection, [Chl-a] and $a_\phi(443)$ standard deviations have not converged yet in both summer and autumn suggesting that the Scotian

412 Shelf is still undergoing significant changes during these two seasons and continuous sampling is required
413 to fully characterize the bio-optical dynamics of the Scotian Shelf.

5 CONCLUSION

414 Our study based on an extensive dataset collected at different times of the year in three oceanographic
415 regimes contributes to the knowledge of bio-optical properties of the Northwest Atlantic and in particular
416 the relationships between phytoplankton biomass and community structure on one side, as indexed by
417 [Chl-a] and [Fucox], and absorption by phytoplankton and non-algal particles on the other side. Using
418 both traditional phytoplankton-based proxies and the *PAAW* index, results show that the characteristics of
419 the phytoplankton and non-algal absorption in the Northwest Atlantic have undergone significant changes
420 over the past 20 years. The adopted *PAAW* index was found to provide equal or better indications of the
421 phytoplankton community compared with metrics that are traditionally measured during oceanographic
422 expeditions. An important aspect in favour of adopting the *PAAW* index is that it is solely based on
423 phytoplankton absorption spectra that are becoming routinely measured in situ by autonomous platforms
424 and profilers. Although additional controlled experiments are needed to evaluate the full potential of
425 *PAAW* to provide insights into phytoplankton community structure, the results of this study suggest that
426 it could be utilized as an efficient integrative index to obtain information on the underwater lightscape
427 characteristics in aquatic ecosystems.

CONFLICT OF INTEREST STATEMENT

428 The authors declare that the research was conducted in the absence of any commercial or financial
429 relationships that could be construed as a potential conflict of interest.

AUTHOR CONTRIBUTIONS

430 E.D. designed the study and assembled the dataset. E.D. and P.M. contributed to data analysis and
431 interpretation. P.M. computed all the statistics and made all the figures and drafted the manuscript. P.M.
432 and E.D. iterated the manuscript.

FUNDING

433 This study was supported by the Atlantic Zone Monitoring Program and Atlantic Zone Offshelf Monitoring
434 Program of the department of Fisheries and Oceans, Canada, in particular, the fieldwork and data analysis
435 in the laboratory. This study was made possible thanks to financial support from the Marine Environmental
436 Observation, Prediction and Response Network (MEOPAR). For further information about MEOPAR, visit
437 www.meopar.ca. This research was supported by the Sentinel North program of Universite Laval through
438 salary support for P. Massicotte, made possible, in part, thanks to funding from the Canada First Research
439 Excellence Fund.

ACKNOWLEDGMENTS

440 We are very grateful to the numerous Chief Scientists, scientists, Captains and crew of the Canadian
441 Coast Guard Ship who have relentlessly relayed over more than 20 years to build this unique dataset of
442 oceanographic properties. We particularly thank the captain and crew of the CCGS Hudson, as this research
443 vessel was used to collect the vast majority of the data presented in the study. The CCGS Hudson was
444 decommissioned in early 2022. We also thank to the chairs of the AZMP and AZOMP programs who have
445 supported this research.

SUPPLEMENTAL DATA

446 Supplementary Material should be uploaded separately on submission, if there are Supplementary Figures,
447 please include the caption in the same file as the figure. LaTeX Supplementary Material templates can be
448 found in the Frontiers LaTeX folder.

DATA AVAILABILITY STATEMENT

449 The datasets [GENERATED/ANALYZED] for this study can be found in the [NAME OF REPOSITORY]
450 [LINK].

REFERENCES

- 451 Aiken, J., Hardman-Mountford, N. J., Barlow, R., Fishwick, J. R., Hirata, T., and Smith, T. J. (2007).
452 Functional links between bio-energetics and bio-optical traits of phytoplankton taxonomic groups: an
453 overarching hypothesis with applications for ocean-colour remote sensing. *J. Plankton Res.* 30, 165–181.
454 doi:10.1093/plankt/fbm098
- 455 Babin, M., Morel, M., Fournier-Sicre, V., Fell, F., and Stramski, D. (2003). Light scattering properties
456 of marine particles in coastal and open ocean waters as related to the particle mass concentration.
457 *Limnol. Oceanogr.* 48, 843–859
- 458 Behrenfeld, M. J., O'Malley, T., R., Siegel, D. A., R., M. C., Sarmiento, J. L., et al. (2006). Climate-driven
459 trends in contemporary ocean productivity. *Nature* 444, 752–755. doi:doi:10.1038/nature05317
- 460 Bidigare, R. R., Morrow, J. H., and Kiefer, D. A. (1989). Derivative analysis of spectral absorption by
461 photosynthetic pigments in the western sargasso sea. *Journal of Marine Research* 47, 323–341
- 462 Brewin, R. J. W., Hardman-Mountford, N. J., Lavender, S. J., Raitsos, D. E., Hirata, T., Uitz, J., et al. (2011).
463 An intercomparison of bio-optical techniques for detecting phytoplankton size class from satellite remote
464 sensing. *Remote Sensing Env.* 115, 325–339. doi:10.1016/j.rse.2010.09.004
- 465 Bricaud, A., Babin, M., Claustre, H., Rase, J., and Tiéche, F. (2010). Light absorption properties
466 and absorption budget of southeast pacific waters. *Journal of Geophysical Research: Oceans* 115.
467 doi:<https://doi.org/10.1029/2009JC005517>
- 468 Bricaud, A., Babin, M., Morel, A., and Claustre, H. (1995). Variability in the chlorophyll-specific
469 absorption coefficients of natural phtoplankton: Analysis and parameterization. *J. Geophys. Res.* 100,
470 13,321–13,332
- 471 Bricaud, A., Claustre, H., and Oubelkheir, K. (2004). Natural variability of phytoplankton absorption
472 in oceanic waters: influence of the size structure of algal populations. *J. Geophys. Res. Oceans* 110.
473 doi:10.1029/2004JC002419
- 474 Bricaud, A., Mejia, C., Blondeau-Patissier, D., Claustre, H., and and. S. Thiria, M. C. (2007). Retrieval
475 of pigment concentrations and size structure of algal populations from their absorption spectra using
476 multilayered perceptrons. *Appl. Opt* 46, 1251–1260
- 477 Bricaud, A., Morel, A., Babin, M., Allali, K., and Claustre, H. (1998). Variations of light absorption
478 by suspended particles with chlorophyll a concentration in oceanic waters: Analysis and implications
479 for bio-optical models. *Journal of Geophysical Research: Oceans* 103, 31033–31044. doi:10.1029/
480 98JC02712
- 481 Casault, B., Johnson, C., Devred, E., Head, E. J. H., Cogswell, A., and Spry, J. (2020). Optical, chemical,
482 and biological oceanographic conditions on the scotian shelf and in the eastern gulf of maine during
483 2019. In *Can. Sci. Advis. Sec. Res. Doc.* (DFO). 64
- 484 Catlett, D. and Siegel, D. A. (2018). Phytoplankton pigment communities can be modeled using uni-
485 que relationships with spectral absorption signatures in a dynamic coastal environment. *Journal of*

- 486 *Geophysical Research: Oceans* 123, 246–264. doi:10.1002/2017JC013195
- 487 Chase, A., Boss, E., Zaneveld, R., Bricaud, A., Claustre, H., Ras, J., et al. (2013). Decomposition of in situ
488 particulate absorption spectra. *Methods in Oceanography* 7, 110–124. doi:<https://doi.org/10.1016/j.mio.2014.02.002>. Special Issue: Advances in Ocean Optical Observing
- 489 Chazottes, A., Bricaud, A., Crépon, M., and Thiria, S. (2006). Statistical analysis of a database of
490 absorption spectra of phytoplankton and pigment concentrations using self-organizing maps. *Appl. Opt.*
491 45, 8102–8115. doi:10.1364/AO.45.008102
- 492 Churilova, T., Suslin, V., Krivenko, O., Efimova, T., Moiseeva, N., Mukhanov, V., et al. (2017). Light
493 absorption by phytoplankton in the upper mixed layer of the black sea: Seasonality and parametrization.
494 *Frontiers in Marine Science* 4. doi:10.3389/fmars.2017.00090
- 495 Ciotti, A. M., Cullen, J. J., and Lewis, M. R. (2002). Assessment of the relationships between domi-
496 nant cell size in natural phytoplankton communities and the spectral shape of absorption coefficient.
497 *Limnol. Oceanogr.* 47, 404–417
- 498 Cleveland, J. S. (1994). The trophic status of various oceanic provinces as revealed by phytoplankton pigment
499 signatures. *Limnol. Oceanogr.* 39, 1206–1210
- 500 Collos, Y., Husseini, J. R., Bec, B., Vaquer, A., Lam, H., Rougier, C., et al. (2005). Pheopigment dynamics,
501 zooplankton grazing rates and the autumnal ammonium peak in a mediterranean lagoon. *Hydrobiologia*
502 550, 83–93. doi:10.1007/s10750-005-4365-1
- 503 Devred, E., Sathyendranath, S., and Platt, T. (2006a). Inversion based on semi-analytical reflectance model.
504 In *Remote sensing of inherent optical properties: Fundamentals, tests of algorithms, and applications*,
505 ed. Z. L. (ed) (Reports of the International Oean-Colour Coordinating Group, No. 5, IOCCG, Dartmouth,
506 Canada)
- 507 Devred, E., Sathyendranath, S., Stuart, V., Maass, H., Ulloa, O., and Platt, T. (2006b). A two-component
508 model of phytoplankton absorption in the open ocean: theory and applications. *J. Geophys. Res.* 111
- 509 Devred, E., Sathyendranath, S., Stuart, V., and Platt, T. (2011). A three component classification of
510 phytoplankton absorption spectra: Application to ocean-color data. *Remote Sensing Env.* 115, 2255–2266.
511 doi:10.1016/j.rse.2011.04.025
- 512 Dutkiewicz, S., Hickman, A. E., Jahn, O., Henson, S., Beaulieu, C., and Monier, E. (2019). Ocean colour
513 signature of climate change. *Nature Communications* 10, 578. doi:10.1038/s41467-019-08457-x
- 514 Duysens, L. M. N. (1956). The flattening of absorption spectrum of suspensions, as compared to that of
515 solutions. *Biochim. Biophys. Acta* 19, 1–12
- 516 Ferreira, A., Ciotti, A. M., C. R. B. Mendes, C. R. B., Uitz, J., and Bricaud, A. (2017). Phytoplankton
517 light absorption and the package effect in relation to photosynthetic and photoprotective pigments in
518 the northern tip of antarctic peninsula. *Journal of Geophysical Research: Oceans* 122, 7344–7363.
519 doi:<https://doi.org/10.1002/2017JC012964>
- 520 Ferreira, A., Stramski, D., Garcia, C. A. E., Garcia, V. M. T., Ciotti, A. M., and Mendes, C. R. B. (2013).
521 Variability in light absorption and scattering of phytoplankton in patagonian waters: Role of community
522 size structure and pigment composition. *Journal of Geophysical Research: Oceans* 118, 698–714.
523 doi:10.1002/jgrc.20082
- 524 Fragoso, G. M., Poulton, A. J., Yashayaev, I., Head, E. J. H., Johnsen, G., and Purdie, D. A. (2018). Diatom
525 biogeography from the labrador sea revealed through a trait-based approach. *Frontiers in Marine Science*
526 5. doi:10.3389/fmars.2018.00297

- 530 Fragoso, G. M., Poulton, A. J., Yashayaev, I., Head, E. J. H., and Purdie, D. A. (2017). Spring phytoplankton
531 communities of the labrador sea (2005–2014): pigment signatures, photophysiology and elemental ratios.
532 *Biogeosciences* 14, 1235–1259. doi:10.5194/bg-14-1235-2017
- 533 Fujiki, T. and Tagushi, S. (2002). Variability in chlorophyll a specific absorption coefficient in marine
534 phytoplankton as a function of cell size and irradiance. *J. Plankton Res.* 24, 859–874
- 535 Gordon, H. R. and McCluney, W. R. (1975). Estimation of the depth of sunlight penetration in the sea for
536 remote sensing. *Appl. Opt.* 14, 413–416
- 537 Head, E. J. H. and Horne, E. P. W. (1993). Pigment transformation and vertical flux in an area of
538 convergence in the north atlantic. *Deep-Sea Res. II* 40, 329–346
- 539 Hieronymi, M., Mueller, D., and Doerffer, R. (2017). The olci neural network swarm (onns): A bio-geo-
540 optical algorithm for open ocean and coastal waters. *Frontiers in Marine Science* 4. doi:10.3389/fmars.
541 2017.00140
- 542 Hirata, T., Aiken, J., Smyth, T. J., Hardman-Mountford, N., and Barlow, R. G. (2008). An absorption model
543 to derive phytoplankton size classes from satellite ocean colour. *Remote Sensing Env.* , 3153–3159
- 544 Hoepffner, N. and Sathyendranath, S. (1991). Effect of pigment composition on absorption properties of
545 phytoplankton. *Mar. Ecol. Prog. Ser.* 73, 11–23
- 546 Hoepffner, N. and Sathyendranath, S. (1993). Determination of the major groups of phytoplankton
547 pigments from the absorption spectra of total particulate matter. *J. Geophys. Res.* 98, 22,789–22,803
- 548 Hoge, F. E. and Lyon, P. E. (1999). Spectral parameters of inherent optical property models: method
549 for satellite retrieval by matrix inversion of an oceanic radiance model. *Appl. Opt.* 38, 1657–1662.
550 doi:10.1364/AO.38.001657
- 551 Kirk, J. T. O. (1976). A theoretical analysis of the contribution of algal cells to the attenuation of light within
552 natural waters. *New Phytologist* 77, 341–358. doi:<https://doi.org/10.1111/j.1469-8137.1976.tb01524.x>
- 553 Kratzer, S. and Moore, G. (2018). Inherent optical properties of the baltic sea in comparison to other seas
554 and oceans. *Remote Sensing* 10. doi:10.3390/rs10030418
- 555 Kyewalyanga, M. N., Platt, T., and Sathyendranath, S. (1997). Estimation of the photosynthetic action
556 spectrum: Implication for primary production models. *Mar. Ecol. Prog. Ser.* 146, 207–223
- 557 Lee, Z. P., Carder, K. L., and Arnone, R. (2002). Deriving inherent optical properties from water color: A
558 multi-band quasi-analytical algorithm for optically deep waters. *Appl. Opt.* 41, 5755–5772
- 559 Leising, A. W., Pierson, J. J., Halsband-Lenk, C., Horner, R., and Postel, J. (2005). Copepod grazing
560 during spring blooms: Does calanus pacificus avoid harmful diatoms? *Progress in Oceanography* 67,
561 384–405. doi:10.1016/j.pocean.2005.09.008. Diatom Blooms and Copepod Responses: Paradigm or
562 Paradox?
- 563 Liu, X., Devred, E., and Johnson, C. (2018). Remote sensing of phytoplankton size class in northwest
564 atlantic from 1998 to 2016: Bio-optical algorithms comparison and application. *Remote. Sens.* 10, 1028.
565 doi:10.3390/rs10071028
- 566 Maritorena, S., Siegel, D. A., and Peterson, A. R. (2002). Optimization of a semi-analytical ocean color
567 model for global-scale applications. *Appl. Opt.* 41, 2705–2713
- 568 Marra, J., Trees, C. C., and O'Reilly, J. E. (2007). Phytoplankton pigment absorption: A strong predictor of
569 primary productivity in the surface ocean. *Deep Sea Research Part I: Oceanographic Research Papers*
570 54, 155–163. doi:<https://doi.org/10.1016/j.dsr.2006.12.001>
- 571 Mascarenhas, V. J., Voss, D., Wollschlaeger, J., and Zielinski, O. (2017). Fjord light regime: Bio-optical
572 variability, absorption budget, and hyperspectral light availability in sognefjord and trondheimsfjord,
573 norway. *Journal of Geophysical Research: Oceans* 122, 3828–3847. doi:<https://doi.org/10.1002/2016JC012610>

- 575 Matsuoka, A., Babin, M., Doxaran, D., Hooker, S. B., Mitchell, B. G., Bélanger, S., et al. (2014). A
576 synthesis of light absorption properties of the arctic ocean: application to semianalytical estimates of
577 dissolved organic carbon concentrations from space. *Biogeosciences* 11, 3131–3147. doi:10.5194/
578 bg-11-3131-2014
- 579 Mitchell, B. G. and Kiefer, B. A. (1984). Determination of absorption and fluorescence excitation spectra
580 for phytoplankton. In *Marine phytoplankton and productivity*, eds. O. Holm-Hansen, L. Bolis, and
581 R. Giles (Berlin Heidelberg: Springer-Verlag). 157–169
- 582 Mitchell, B. G. and Kiefer, B. A. (1988). Variability in pigment specific particulate fluorescence and
583 absorption spectra in the northeast Pacific Ocean. *Deep-Sea Res.* 28, 1375–1393
- 584 Mobley, C. D. (1994). Optical properties of water. In *Light and Water: Radiative Transfer in Natural
585 Waters*, eds. O. Holm-Hansen, L. Bolis, and R. Giles (London: Academic Press). 61–142
- 586 Moran, M. A. and Zepp, R. G. (1997). Role of photoreactions in the formation of biologically labile
587 compounds from dissolved organic matter. *Limnology and Oceanography* 42, 1307–1316. doi:<https://doi.org/10.4319/lo.1997.42.6.1307>
- 588 Morel, A. (1978). Available, usable, and stored radiant energy in relation to marine photosynthesis. *Deep
589 Sea Research* 25, 673–688. doi:[https://doi.org/10.1016/0146-6291\(78\)90623-9](https://doi.org/10.1016/0146-6291(78)90623-9)
- 590 Morel, A. and Bricaud, A. (1981). Theoretical results concerning light absorption in a discrete medium,
591 and application to specific absorption of phytoplankton. *Deep Sea Res.* 28, 1375–1393
- 592 Morel, A. and Prieur, L. (1977). Analysis of variation in ocean color. *Limnol. Oceanogr.* 22, 709–722
- 593 Nagasaki, K. (2008). Dinoflagellates, diatoms, and their viruses. *Journal of microbiology (Seoul, Korea)*
594 46, 235–43. doi:10.1007/s12275-008-0098-y
- 595 Nardelli, S. C. and Twardowski, M. S. (2016). Assessing the link between chlorophyll concentration and
596 absorption line height at 676 nm over a broad range of water types. *Opt. Express* 24, A1374–A1389.
597 doi:10.1364/OE.24.0A1374
- 598 Oubelkheir, K., Claustre, H., Bricaud, A., and Babin, M. (2007). Partitioning total spectral absorption in
599 phytoplankton and colored detrital material contributions. *Limnology and Oceanography: Methods* 5,
600 384–395. doi:<https://doi.org/10.4319/lom.2007.5.384>
- 601 Pepin, P., Petrie, B., Therriault, J.-C., Narayanan, S., Harrisson, W., Frank, K., et al. (2005). The atlantic
602 zone monitoring program (azmp): Review of 1998–2003. *Can. Tech. Rep. Hydrogr. Ocean Sci.* 242, 57
- 603 Platt, T. and Gallegos, C. L. (1980). *Modelling Primary Production* (Boston, MA: Springer US). 339–362.
604 doi:10.1007/978-1-4684-3890-1_19
- 605 Pérez, G. L., Galí, M., Royer, S.-J., Gerea, M., Ortega-Retuerta, E., Gasol, J. M., et al. (2021). Variability
606 of phytoplankton light absorption in stratified waters of the nw mediterranean sea: The interplay between
607 pigment composition and the packaging effect. *Deep Sea Research Part I: Oceanographic Research
608 Papers* 169, 103460. doi:<https://doi.org/10.1016/j.dsr.2020.103460>
- 609 Roesler, C. S. and Barnard, A. H. (2013). Optical proxy for phytoplankton biomass in the absence
610 of photophysiology: Rethinking the absorption line height. *Methods in Oceanography* 7, 79–94.
611 doi:10.1016/j.mio.2013.12.003. Special Issue: Advances in Ocean Optical Observing
- 612 Sathyendranath, S., Watts, L., Devred, E., Platt, T., Caverhill, C., and Maass, H. (2004). Discrimination of
613 diatoms from other phytoplankton using ocean-colour data. *Mar. Ecol. Prog. Ser.* 272, 59–68
- 614 Shuman, F. R. and Lorenzen, C. J. (1975). Quantitative degradation of chlorophyll by a marine herbivore.
615 *Limnology and Oceanography* 20, 580–586. doi:<https://doi.org/10.4319/lo.1975.20.4.0580>
- 616 Sosik, H. M. and Mitchell, B. G. (1992). A comparison of particulate absorption properties between high-
617 and mid-latitude surface waters. *Antarctic. J. United States* 27, 162–164

- 619 Staehr, A., Markager, S., and Sand-Jensen, K. (2004). Pigment specific in vivo light absorption of
620 phytoplankton from estuarine, coastal and oceanic waters. *Marine Ecology Progress Series* 275,
621 115–128. doi:10.3354/meps275115
- 622 Stramski, D., Reynolds, R. A., Kaczmarek, S., Uitz, J., and Zheng, G. (2015). Correction of pathlength
623 amplification in the filter-pad technique for measurements of particulate absorption coefficient in the
624 visible spectral region. *Appl. Opt.* 54, 6763–6782. doi:10.1364/AO.54.006763
- 625 Stuart, V., Sathyendranath, S., Head, E. J. H., Platt, T., Irwin, B. D., and Maas, H. (2000). Bio-optical
626 characteristics of diatom and prymnesiophyte populations in the Labrador Sea. *Mar. Ecol. Prog. Ser.*
627 201, 91–106
- 628 Teegarden, G. J., Campbell, R. G., and Durbin, E. G. (2001). Zooplankton feeding behavior and particle
629 selection in natural plankton assemblages containing toxic *Alexandrium* spp. *Marine Ecology Progress Series*
630 Series 218, 213–226. doi:10.3354/meps218213
- 631 Therriault, J.-C., Petrie, B., P. Pépin, J. G., Gregory, D., Helbig, J., Herman, A., et al. (1998). Proposal for
632 a northwest atlantic zonal monitoring program. In *Can. Tech. Rep. Hydrogr. Ocean Sci.* (DFO), vol. 194.
633 vii+57
- 634 Trees, C. C., Clark, D. K., Bidigare, R. R., Ondrusek, M. E., and Mueller, J. L. (2000). Accessory
635 pigments versus chlorophyll *a* concentrations within the euphotic zone: An ubiquitous relationship.
636 *Limnol. Oceanogr.* 45, 1130–1143
- 637 Uitz, J., Claustre, H., Morel, A., and Hooker, S. B. (2006). Vertical distribution of phytoplankton
638 communities in open ocean: An assessment based on surface chlorophyll. *J. Geophys. Res.* 111.
639 doi:10.1029/2005jc003207
- 640 Vandermeulen, R. A., Mannino, A., Craig, S. E., and Werdell, P. J. (2020). 150 shades of green: Using the
641 full spectrum of remote sensing reflectance to elucidate color shifts in the ocean. *Remote Sensing of*
642 *Environment* 247, 111900. doi:<https://doi.org/10.1016/j.rse.2020.111900>
- 643 Vidussi, F., Claustre, H., Manca, B. B., Luchetta, A., and Marty, J. C. (2001). Phytoplankton pigment
644 distribution in relation to upper thermocline circulation in the eastern Mediteranean Sea during winter.
645 *J. Geophys. Res.* 106, 19,939–19,956
- 646 Vishnu, P., Shaju, S., Tiwari, S., Menon, N., Nashad, M., Joseph, C. A., et al. (2018). Seasonal variability
647 in bio-optical properties along the coastal waters off cochin. *International Journal of Applied Earth*
648 *Observation and Geoinformation* 66, 184–195. doi:10.1016/j.jag.2017.12.002
- 649 Werdell, J., Mckinna, L., Boss, E., Ackleson, S., Craig, S., W. Gregg, W., et al. (2018). An overview of
650 approaches and challenges for retrieving marine inherent optical properties from ocean color remote
651 sensing. *Progress in Oceanography* 160. doi:10.1016/j.pocean.2018.01.001
- 652 Williams, G. N., Larouche, P., Dogliotti, A. I., and Latorre, M. P. (2018). Light absorption by phytoplankton,
653 non-algal particles, and dissolved organic matter in san jorge gulf in summer. *Oceanography* 31, 40–49.
654 doi:10.5670/oceanog.2018.409
- 655 Wu, Y., Platt, T., Tang, C., Sathyendranath, S., Devred, E., and Gu, S. (2008). A summer phytoplankton
656 bloom triggered by high wind events in the labrador sea, july 2006. *Geophys. Res. Lett.* 35, doi:
657 10.1029/2008GL033561
- 658 Yashayaev, I., Peterson, I., and Wang, Z. (2021). Meteorological, sea ice, and physical oceanographic
659 conditions in the labrador sea during 2018. In *Can. Sci. Advis. Sec. Res. Doc.* (DFO), vol. 42. 26
- 660 Zhang, Y., Wang, G., Sathyendranath, S., Xu, W., Xiao, Y., and Jiang, L. (2021). Retrieval of phytoplankton
661 pigment composition from their in vivo absorption spectra. *Remote Sensing* 13. doi:10.3390/rs13245112

TABLES

Season	N	[Chl-a]	[Fuco]	$a_\phi(443)$	$a_\phi^*(443)$	$a_{NAP}(443)$	S_{NAP}	$PAAW$
All data	2267	1.53 (0.06 – 17.5)	0.41 (0 – 6.68)	0.048 (0.004 – 0.231)	0.055 (0.004 – 0.290)	0.0065 (0.0002 – 0.1384)	0.0115 (0.0001 – 0.0415)	478.5 (456.5 – 500.5)
Scotian Shelf								
Spring	781	2.70 (0.102 – 13.6)	0.89 (0.000 – 6.68)	0.049 (0.004 – 0.216)	0.0297 (0.004 – 0.1636)	0.009 (0.0002 – 0.0378)	0.0124 (0.0018 – 0.0275)	482.5 (461.6 – 500.5)
Summer	36	0.32 (0.093 – 0.882)	0.03 (0.000 – 0.131)	0.022 (0.009 – 0.057)	0.0781 (0.0321 – 0.133)	0.0042 (0.001 – 0.0132)	0.0118 (0.0062 – 0.0195)	470.2 (462.3 – 480.1)
Autumn	781	0.83 (0.080 – 4.13)	0.13 (0.000 – 1.68)	0.050 (0.007 – 0.177)	0.0724 (0.0048 – 0.2896)	0.0065 (0.0004 – 0.0314)	0.01 (0.0004 – 0.02)	477.5 (456.5 – 487.9)
Winter	74	0.68 (0.211 – 1.59)	0.16 (0.053 – 0.517)	0.032 (0.009 – 0.064)	0.0493 (0.0212 – 0.1463)	0.0078 (0.0007 – 0.0178)	0.0088 (0.006 – 0.0167)	480.9 (471.7 – 485.4)
Northwest Atlantic Basin								
Spring	313	1.80 (0.091 – 10.4)	0.47 (0.000 – 5.37)	0.051 (0.008 – 0.176)	0.0421 (0.0063 – 0.1724)	0.0051 (0.0005 – 0.0419)	0.0131 (0.0001 – 0.0403)	479.0 (460.7 – 496.1)
Summer	58	0.21 (0.090 – 0.553)	0.03 (0.000 – 0.168)	0.017 (0.007 – 0.037)	0.0890 (0.0598 – 0.1373)	0.0033 (0.0009 – 0.0095)	0.0129 (0.005 – 0.0175)	469.1 (460.2 – 486.5)
Autumn	369	0.400 (0.060 – 2.19)	0.040 (0.000 – 0.892)	0.028 (0.009 – 0.081)	0.0838 (0.0246 – 0.2305)	0.0036 (0.0002 – 0.0184)	0.011 (0.003 – 0.0284)	472.1 (459.5 – 485.8)
Winter	45	0.87 (0.531 – 2.03)	0.16 (0.031 – 0.796)	0.032 (0.016 – 0.054)	0.0389 (0.0204 – 0.0607)	0.0037 (0.0006 – 0.0082)	0.0111 (0.0069 – 0.0186)	479.4 (473.8 – 484.3)
Labrador Sea								
Spring	504	2.73 (0.076 – 17.5)	0.72 (0.000 – 4.73)	0.063 (0.004 – 0.224)	0.0363 (0.0069 – 0.1428)	0.0075 (0.0004 – 0.1384)	0.0134 (0.0026 – 0.0415)	481.5 (460.7 – 498.1)
Summer	275	1.99 (0.10 – 8.48)	0.67 (0.000 – 4.43)	0.061 (0.012 – 0.231)	0.0489 (0.0081 – 0.2402)	0.0068 (0.0011 – 0.0289)	0.0106 (0.0012 – 0.0297)	477.7 (465.0 – 494.4)
Autumn	24	0.88 (0.225 – 3.19)	0.26 (0.000 – 1.41)	0.038 (0.014 – 0.093)	0.0538 (0.0188 – 0.1069)	0.0031 (0.0004 – 0.0065)	0.0163 (0.01 – 0.0228)	478.7 (472.9 – 492.7)
Winter	19	0.19 (0.093 – 0.321)	0.05 (0.017 – 0.155)	0.009 (0.004 – 0.014)	0.0471 (0.0377 – 0.0521)	0.0017 (0.001 – 0.0037)	0.0121 (0.0109 – 0.0139)	477.8 (475.4 – 480.2)

Table 1. Mean values and range of variations (min – max) of [Chl-a], [Fucox], $a_\phi(443)$, $a_\phi^*(443)$, $a_{NAP}(443)$, S_{NAP} and $PAAW$ for the Scotian Shelf, Northwest Atlantic and Labrador Sea in spring, summer, autumn and winter. Note that N correspond to the number of samples collected and the actual number of a given properties might be lower after quality control or due to mishandling during data processing.

Dataset	slope	p-value	R^2
All	0.083	NS	0.11
Regions			
Scotian Shelf	0.107	NS	0.05
NAB	0.136	NS	0.10
Labrador Sea	0.082	NS	0.08
Regions in Spring			
Scotian Shelf	0.382	< 0.05	0.28
NAB	0.229	< 0.05	0.36
Labrador Sea	0.347	< 0.05	0.32
Regions in Autumn			
Scotian Shelf	-0.155	< 0.05	0.27
NAB	-0.348	< 0.05	0.61

Table 2. Slope, p-value and correlation coefficient (R^2) of the linear regression of *PAAW* against time in year.

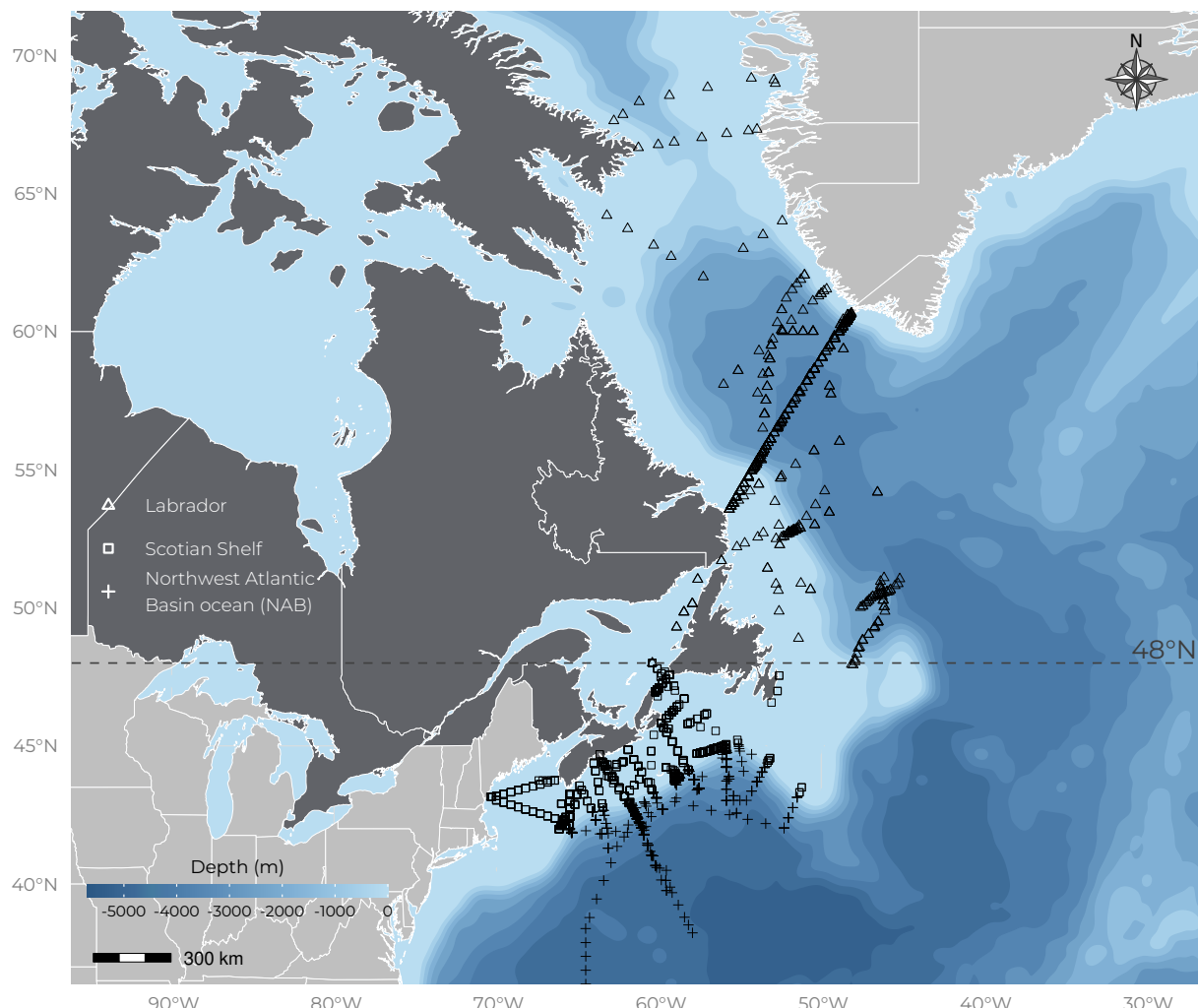
FIGURE CAPTIONS

Figure 1. Location of Samplings. The blue background indicate the bathymetry (see colorbar in bottom left panel). Dark grey corresponds to Canada and light Grey corresponds to other countries (i.e., United States of America and Denmark)

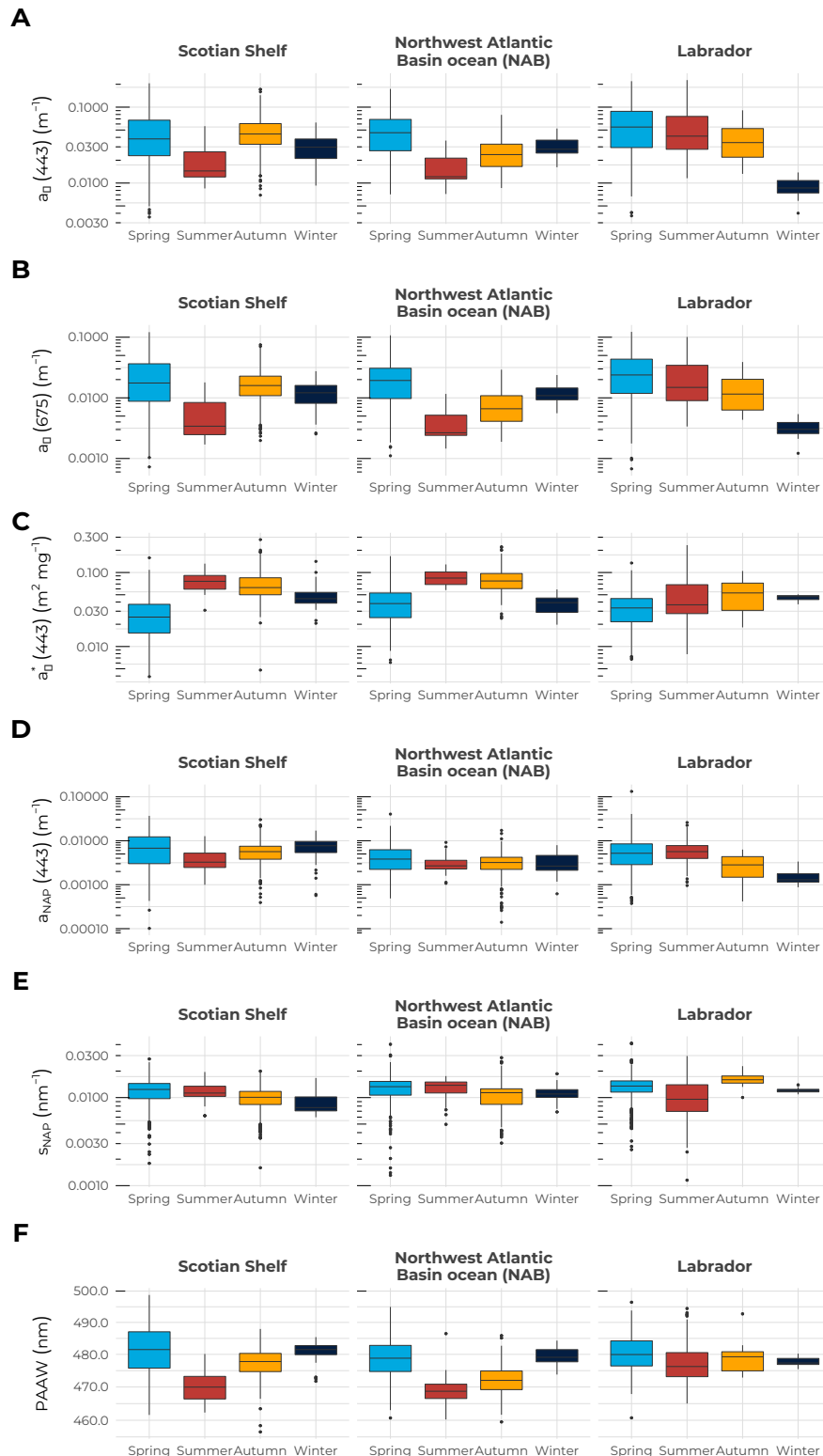


Figure 2. Mean and one standard deviation (i.e., boxplot) of A) $a_\phi(443)$, B) $a_\phi(675)$, C) $a_\phi^*(443)$, D) $a_{NAP}(443)$, E) S_{NAP} and F) PAAW for the Scotian Shelf (left column), Northwest Atlantic Ocean (middle column) and Labrador Sea (right column). In each panel, the blue, red, yellow and black boxes correspond to the spring, summer, autumn and winter respectively.

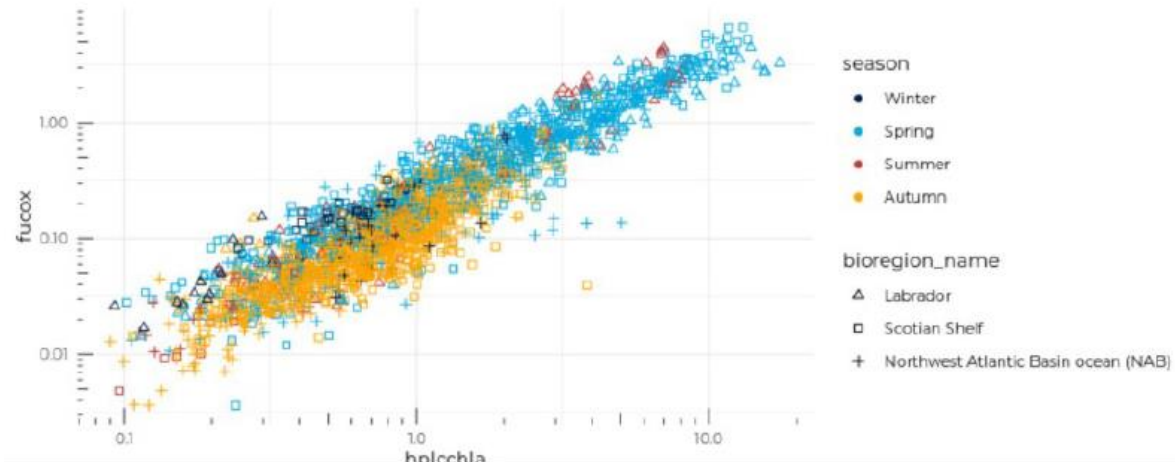


Figure 3. [Fucox] as a functin of [Chl-a]. Symbols are colour coded according to season as in Figure 2

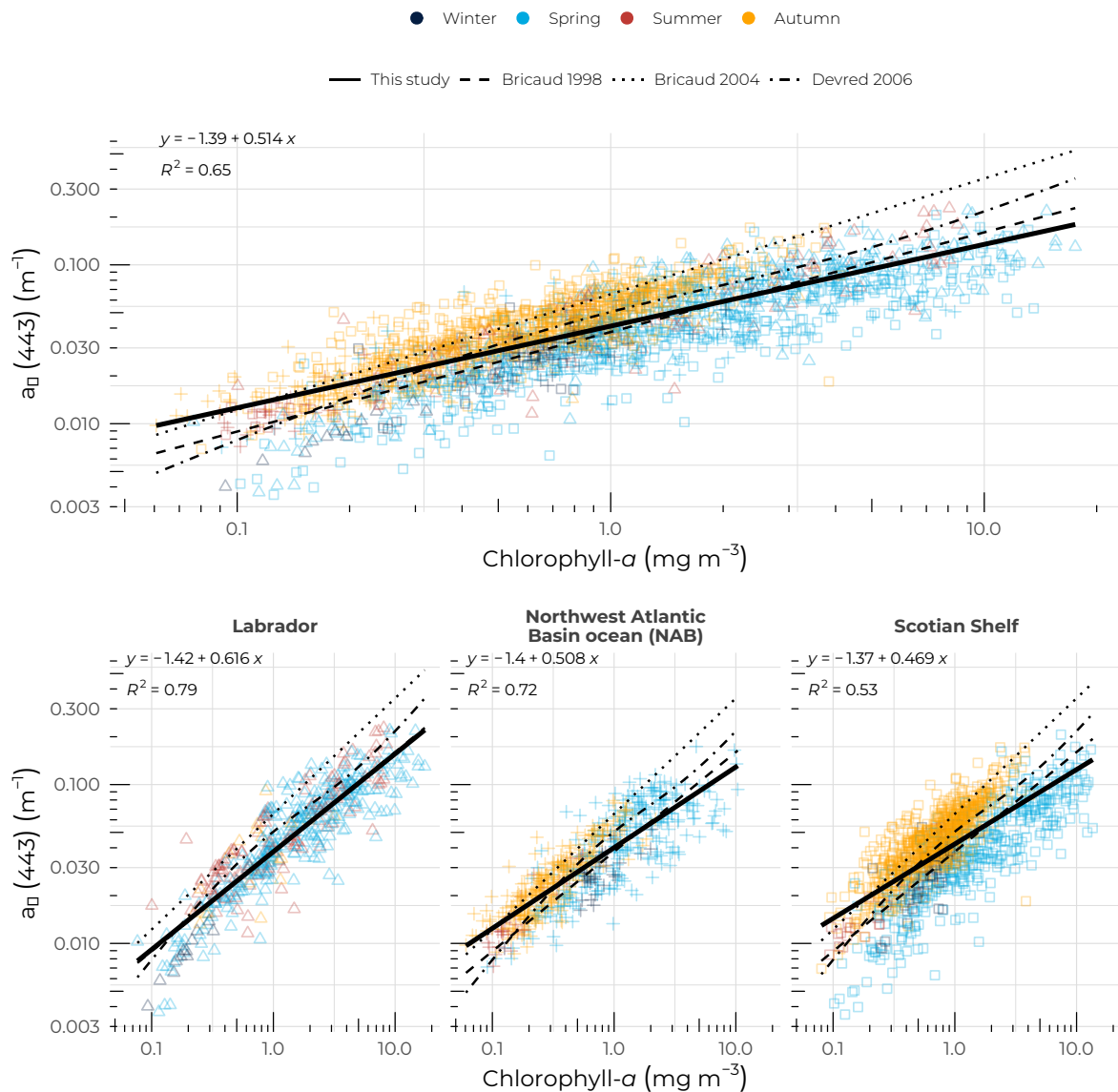


Figure 4. Phytoplankton absorption coefficient at 443 nm, $a_\phi(443)$, as a function of [Chl-a] for A) the entire dataset, B) the Scotian Shelf, C) the Northwest Atlantic Basin and D) the Labrador Sea. The solid black lines correspond to the power law fit (Equation 3.2), the long-dashed, short-dashed and dotted-dashed lines correspond to Bricaud et al. (1998), Bricaud et al. (2004) and Devred et al. (2006b) models respectively. Symbols are colour coded according to season as in Figure 2

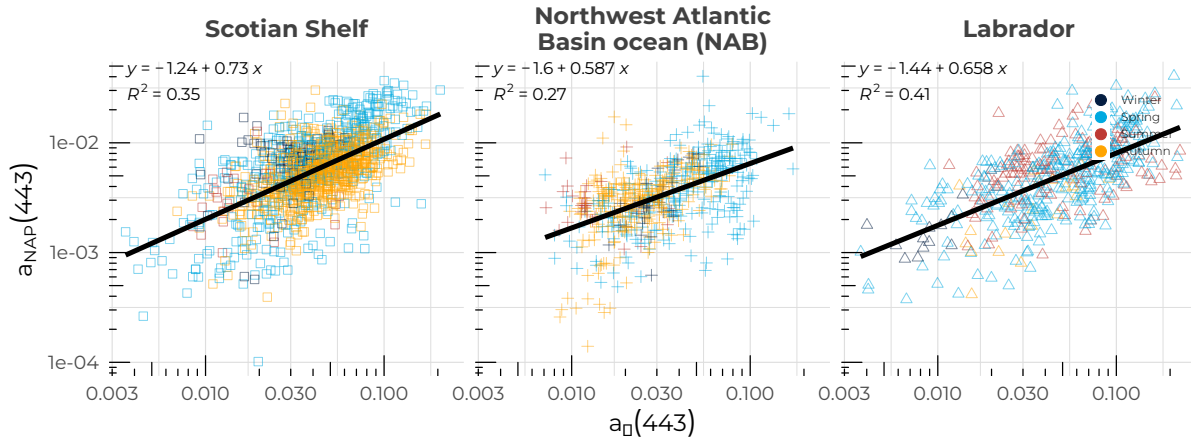


Figure 5. I dont know what you mean. In the legend you talk about chl and this figure do not show cha. Also, I do not know what is fig 5b, you changed the figure order. Non-algal particulate absorption coefficient at 443 nm, $a_{NAP}(443)$, as a function of [Chl-a] for A) the entire dataset, B) the Scotian Shelf, C) the Northwest Atlantic Basin and D) the Labrador Sea. The solid black lines correspond to the power law fit (Equation 3.2), the long-dashed, short-dashed and dotted-dashed lines correspond to Bricaud et al. (1998), Bricaud et al. (2004) and Devred et al. (2006b) models respectively. Symbols are colour coded according to season as in Figure 2

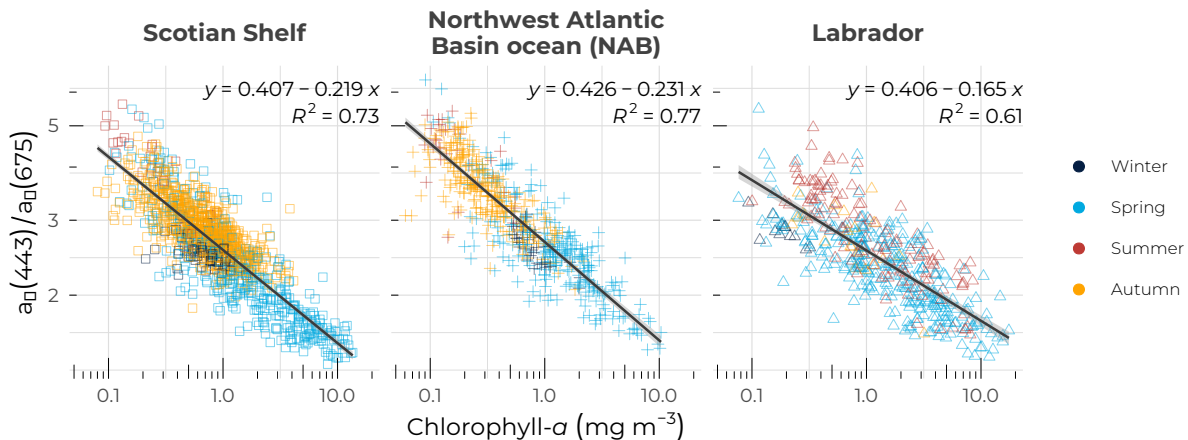


Figure 6. Ratio of $a_\phi(443)$ to $a_\phi(675)$ as a function of [Chl-a] for the Scotian Shelf (left), Northwest Atlantic Basin (middle) and Labrador Sea (right). Symbols are colour coded according to season as in Figure 2

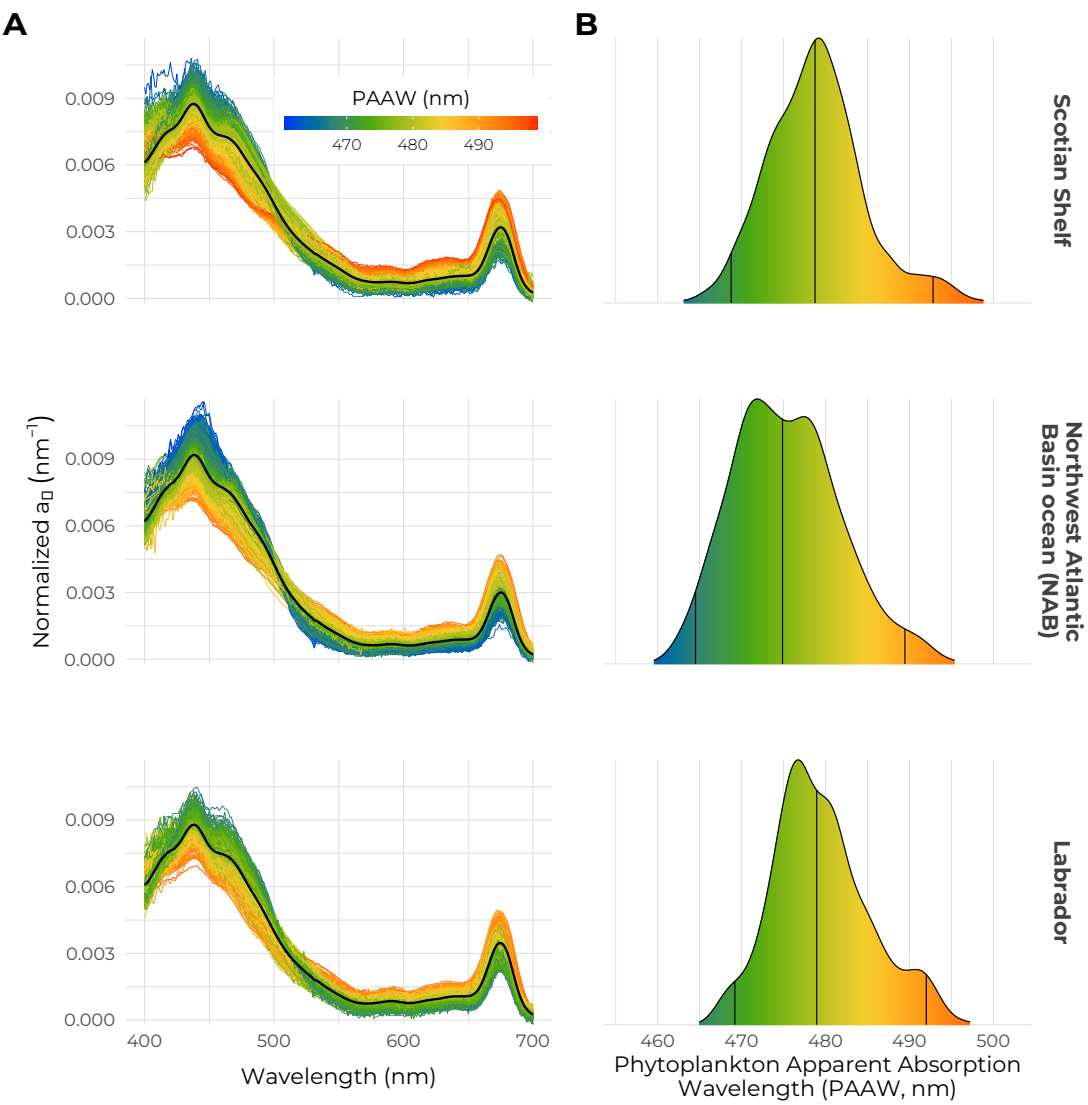


Figure 7. A) Phytoplankton absorption spectra and B) distribution of the *PAAW* for the Scotian Shelf (top), NAB (middle) and Labrador Sea (bottom), the color bar indicate the *PAAW* values in all panels.

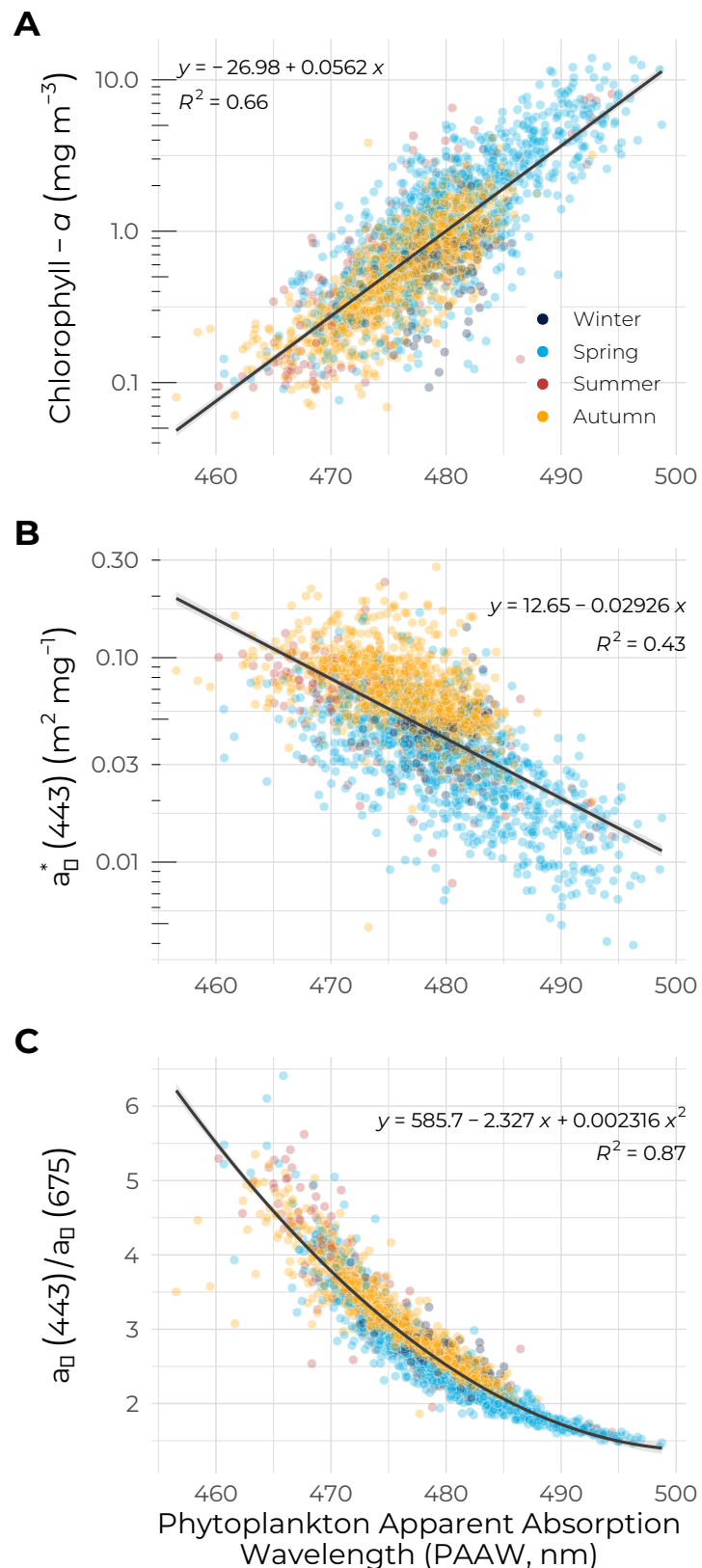


Figure 8. A) [Chl-a], B) $a_\phi^*(443)$ and C) $a_\phi(443) : a_\phi(675)$ as a function of PAAW for the entire dataset

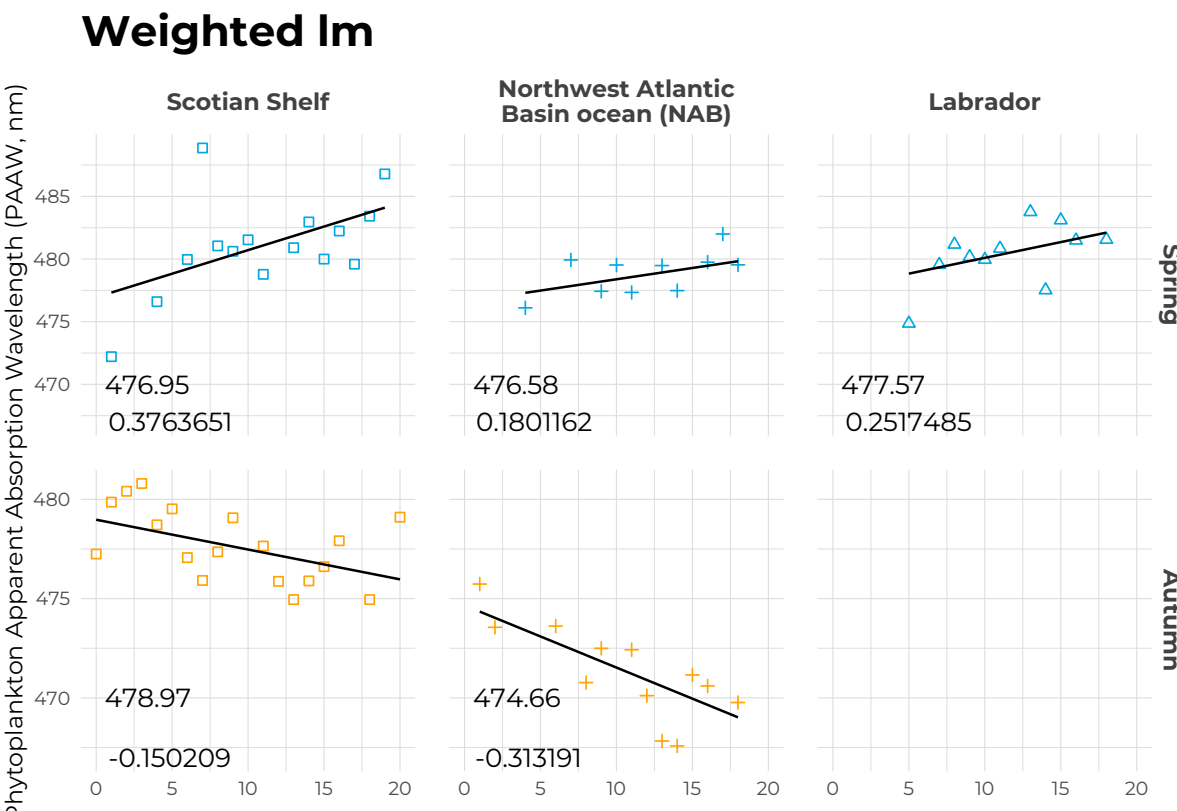


Figure 9. Seasonal trends in *PAAW* for spring (top panels) and autumn (bottom panels) for the Scotian Shelf (left), NAB (middle) and Labrador Sea (right). The black solid lines correspond to the linear regression of *PAAW* against time with the coefficient and R^2 indicated in each panel. Symbols are colour coded according to season as in Figure 2

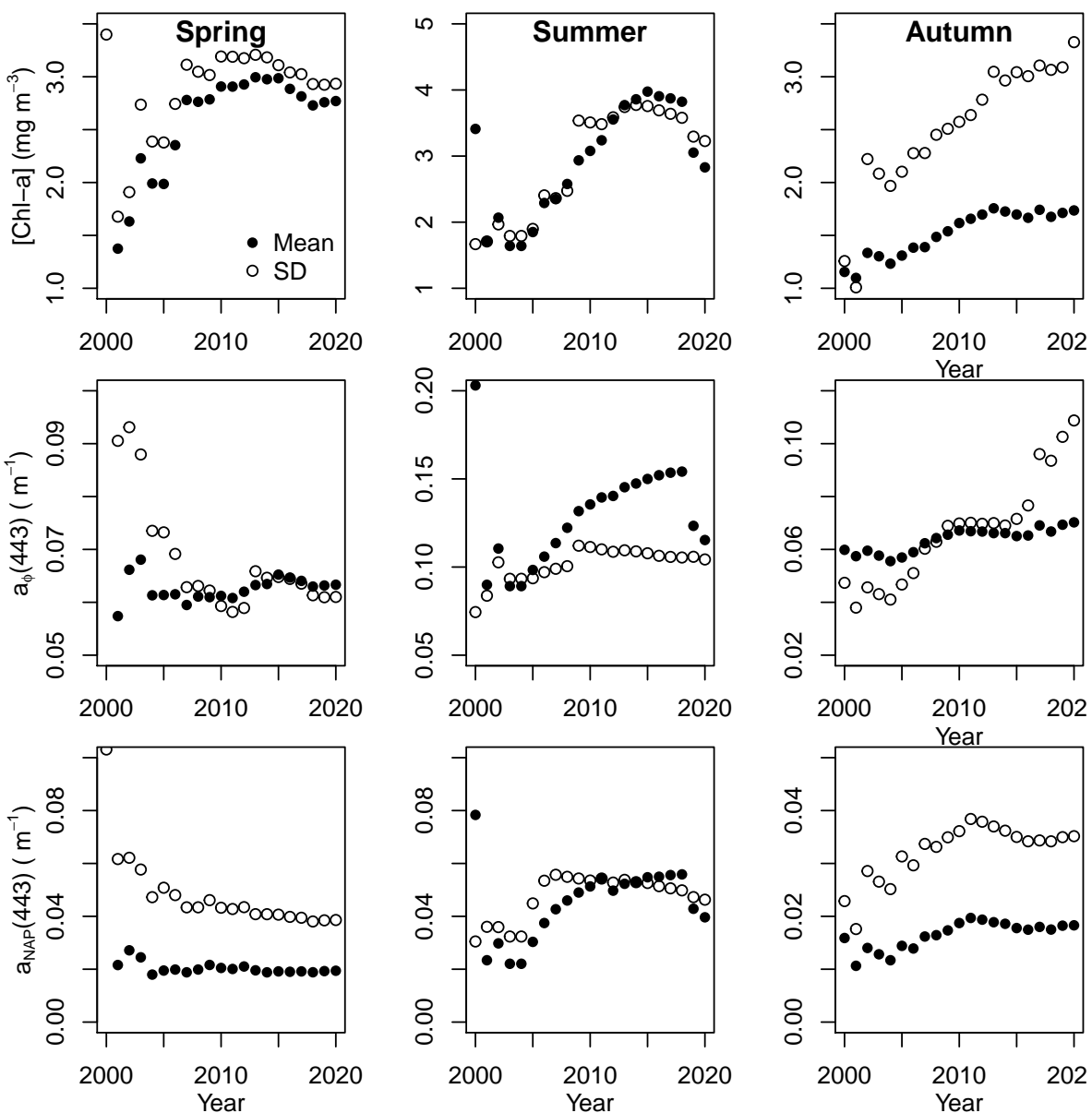


Figure 10. Mean (solid black circles) and standard deviation (open black circle) as a function of time for [Chl-a] (top), $a_{\phi}(443)$ (middle) and $a_{NAP}(443)$ (bottom) (you should use text mode to write NAP instead of math mode, it does not look good) in spring (left column), summer (middle column) and autumn (right column on the Scotian Shelf